TECHNICAL UNIVERSITY OF CLUJ-NAPOCA

ACTA TECHNICA NAPOCENSIS

Series: Applied Mathematics, Mechanics, and Engineering
Vol. 69, Issue I, March, 2026

IN VITRO CORROSION BEHAVIOR OF A BIODEGRADABLE ZnMg-Ti ALLOY IN DPBS

Ramona CIMPOEȘU, Romeu CHELARIU, Alexandra-Tamara ȘUTIC, Adrian ALEXANDRU, Ana-Maria ROMAN, Gheorghe BĂDĂRĂU, Raluca-Maria FLOREA, Cătălin-Andrei ȚUGUI, Mihai-Adrian BERNEVIG, Marius TELIȘCĂ, Nicanor CIMPOEȘU

Abstract: *Biodegradable alloys are increasingly being used in the medical field for procedures that do not require permanent implants or extensive healing times. The slower degradation rate of zinc-based alloys compared to magnesium-based alloys enables the solution of a wider range of medical concerns. After obtaining a ZnMgTi alloy by classical casting in an induction furnace, its behavior in Dulbecco's Phosphate Buffered Saline (DPBS) was studied. Characterizing the interaction between the alloy and DPBS led to possible explanations for the alloy's corrosion behavior. These hypotheses were confirmed by analyzing the solution's pH evolution, as well as by conducting chemical analyses using X-ray energy spectroscopy (EDS) and scanning electron microscopy (SEM), and by assessing mass loss after immersion.*
Key words: *biodegradable ZnMgTi alloy, microstructure, corrosion behavior.*

1. INTRODUCTION

Among the systems of interest in current research on biodegradable metallic materials for medical applications are zinc (Zn)-based alloys modified with titanium (Ti) and magnesium (Mg), as well as ternary combinations (ZnMgTi), which promise good biocompatibility and suitable mechanical properties [1-4]. The applicability of these materials is dependent upon their corrosion behavior, which in turn determines the rate and process of biodegradation [5-8].

García-Mintegui et al. [9] investigated the corrosion mechanisms and performance of Zn-0.5 Mg and Zn-1 Mg alloys for biodegradable cardiovascular stents. They discovered that adding 1 wt% Mg refined the zinc microstructure, raising the tensile strength to 222 MPa (YS) and 260 MPa (UTS), while also stabilizing degradation in Hank's solution through the formation of uniform corrosion products. Galvanic corrosion between the Zn matrix and Mg_2Zn_{11} secondary phases resulted in a controlled degradation rate of approximately 50 µm/year, which is ideal for stents [9].

Wang et al. [10] investigated the properties of Zn-xTi binary alloys for orthopedic applications. They found that increasing the percentage of added titanium (Ti) from 0.05 to 0.3 wt% increased the corrosion rate in Hank's solution from 47.5 to 57.9 µm/year by forming a protective oxide layer and improving wear resistance. Controlled degradation resulted in the release of non-toxic products (ZnO and $Zn(OH)_2$) [10].

Zhang et al. [1] studied the corrosion behavior and other properties of a Zn-3Mg-1Ti alloy intended for use in biodegradable implants. Combining Mg (3%) and Ti (1%) resulted in a refined microstructure, which enhanced the mechanical strength (625.1 MPa, 226.4 HV) due to the strong combination of the Mg_2Zn_{11} and $TiZn_{16}$ phases. This combination also reduced the corrosion rate to 78.5 µm/y in Hank's solution. Titanium (Ti) inhibited galvanic corrosion between the zinc (Zn) matrix and Mg_2Zn_{11} phases by forming stable oxides, ensuring uniform degradation. Cytotoxicity tests revealed that the alloy is more biocompatible than binary alloys [1].

By controlling the chemical composition (the proportion of Mg and Ti), both the degradation

Received: 26.01.26; **Similarities**: 12.02.26: **Reviewed**: 26.01./ 26.01.26: **Accepted** 19.03.26.

rate and corrosion resistance of zinc-based alloys can be adjusted [11-16], making them versatile materials for applications in aggressive environments, including the medical field.

The chemical composition of the new ZnMgTi alloy under investigation in the present study promises superior mechanical strength and controlled degradation due to the Ti-rich and Mg-rich phases [1]. The performance of the alloy under consideration exceeds that of other Zn-based alloys, including binary Zn-Mg and Zn-Ti alloys, as reported in the available literature [8,11].

2. EXPERIMENTAL MATERIALS AND SET-UP

A ZnMgTi alloy was produced by casting in an induction furnace using high-purity zinc (99.995%), magnesium (99.9%), and titanium (99.9%). Initially, ZnMg and ZnTi pre-alloys were obtained, and finally, the ZnMgTi alloy was produced (in total, about five melting and homogenization operations were performed).

Table 1

The initial chemical composition of the experimental ZnMgTi alloy.

Area	Zn		Mg		Ti	
	wt%	at%	wt%	at%	wt%	at%
4 mm² area	96	91	3.5	8.9	0.5	0.7
EDS err %	0.6		0.58		0.05	

St.dev: Zn:±1.5; Mg:±0.2; Ti:±0.05

The alloy's chemical composition (an average value obtained from five chemical composition determinations), shown in Table 1, was found to be 0.5% Ti and 3.5% Mg by weight. This composition was projected according to literature and binary diagram analysis (Zn-Mg, Zn-Ti, and Ti-Mg).

The corrosion resistance of the experimental alloy was evaluated through immersion experiments and by measuring the pH variation of the solution over 72 hours [3, 4]. Dulbecco's phosphate-buffered saline (without Ca or Mg, code: 17-515Q) (SAFC Bioscience LTD, Hampshire, UK): 10xDPBS (chemical composition: KCl: 0.2; KH_2PO_4: 0.2; NaCl: 8.0; and NaH_2PO_4 (anhydrous): 1.15) was used for the tests. The pH of the solution in contact with the ZnMgTi alloy was monitored minute-by-minute for three days using a Hanna pH meter and a temperature probe to correlate the chemical interactions occurring at the alloy's surface with the formation of compounds passing into the solution and changing its pH.

The surface condition after immersion was investigated using scanning electron microscopy (SEM) with a Vega Tescan LMH II tungsten filament (powered at 30 kV) with a working distance of 15.5 mm and a secondary electron (SE) detector in forward vacuum [17,18]. The surface's chemical composition was determined using X-ray energy dispersive spectroscopy (EDS) analysis with a Bruker 6i10 EDS detector, Automatic Analysis mode, and Mapping Analysis mode with Esprit 2.2 software [19,20].

3. EXPERIMENTAL RESULTS

The samples were immersed in DPBS at 37 °C in a thermostatically controlled chamber for 3 days (72 hours). In this experiment, no pH adjustment of the solution was performed, and the behavior of the alloy in direct contact with the solution was observed. The sample was preliminarily polished to a mirror-like finish. An increase in the solution's pH was observed from the first hours of immersion (Figure 1(a)), followed by stabilization of the pH, which correlated with the formation of an oxide layer on the alloy's surface. Figure 1(b) illustrates the estimated variation in pH of DPBS over three days during ZnMgTi alloy immersion, taking into account chemical reactions and experimental observations after the initial abrupt increase.

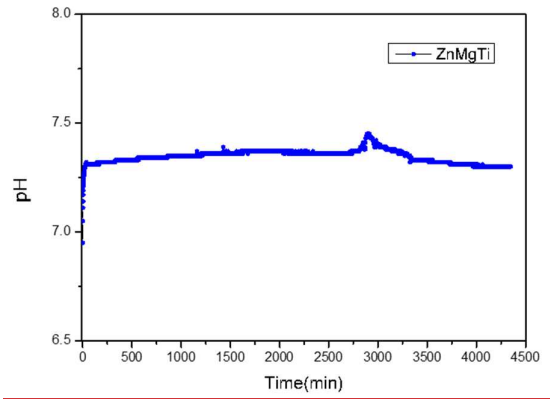

(a)

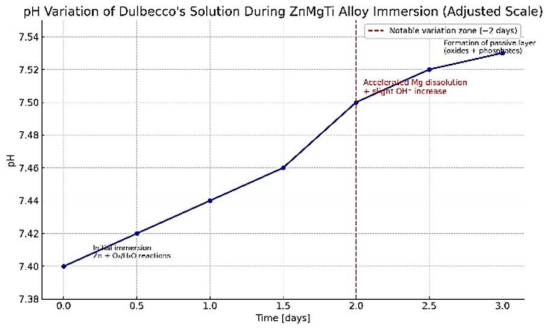

(b)

Fig. 1. pH variation of DPBS over 72 hours of immersion: (a) pH values recorded over 72 hours; (b) pH values — adjusted scale.

During the early stage (0-1.5 days), a moderate increase in pH occurs due to the initial corrosion of Zn and the release of OH^- by oxygen reduction. On the second day of immersion (indicated by the dotted red line), there is a marked change in pH, indicating an acceleration of Mg dissolution and the generation of more OH^-, which sharply raises the pH. From days two to three, the system begins to stabilize as a passive oxide/phosphate layer covers the surface, and the reactions slow down. The pH gradually rises in the first part of the experiment, causing slight alkalinization of the solution, followed by slight stabilization or plateauing. Corrosion of Zn and Mg generates metal ions and OH^- in anodic reactions (metal oxidation): $Zn \rightarrow Zn^{2+} + 2e^-$ and $Mg \rightarrow Mg^{2+} + 2e^-$. In a cathodic reaction in neutral or acidic environments, dissolved oxygen reacts with the metal surface: $O_2 + 2H_2O + 4e^- \rightarrow 4OH^-$. The OH^- ions generated in this reaction cause an increase in the solution's pH.

The sudden acceleration of magnesium (Mg) dissolution occurs because Mg is more reactive than zinc (Zn) and may initially be protected by an oxide layer or slight passivation. After a certain amount of time (~2 days), however, this layer can be disrupted, leading to faster dissolution. The reaction $Mg + 2H_2O \rightarrow Mg(OH)_2 + H_2$ releases magnesium hydroxide, which contributes to the increase in pH. After corroding for a period of time, more stable phosphates and oxides (e.g., $Zn_3(PO_4)_2$) begin to form. These phosphates and oxides can lead to the consumption of H^+ ions from the solution through precipitation or complexation reactions, which also favors an increase in pH. A change in the reaction rate can occur due to the partial saturation of the solution. As the concentration of Zn^{2+} and Mg^{2+} increases in the solution, changes in chemical equilibrium and the formation of solids can occur.

An apparent increase in mass after immersion is shown in Table 2 after one and three days. This indicates the formation of solid layers on the surface, such as metal oxides (e.g., ZnO, MgO) and phosphates (e.g., $Zn_3(PO_4)_2$, $Mg_3(PO_4)_2$), as well as possible ionic adsorbates from the DPBS (e.g., Na^+, P, Cl^-). After ultrasonic cleaning in isopropyl alcohol, the sample's mass returns nearly to its initial value due to the products formed during this period being weakly bound to the surface and fragile or weakly adherent, making them easily removable.

Table 2

Mass loss after immersion in DPBS for 1, 3 and 20 days.

Immersion time	1 day	3 days	20 days
Initial mass (mg)	2737	2566.3	3554.4
After immersion (mg)	2738.4 (+1.4)	2567.4 (+1.1)	3570.8 (+16.4)
After ultrasound (mg)	2737.3 (+0.3)	2566.5 (+0.2)	3559.1 (+4.7)

cylindrical sample dimensions: 10 mm diameter; 4 mm height

There was nearly no significant mass loss in the first three days. This suggests a corrosion process with rapid passivation rather than massive dissolution. After 20 days, the mass increased visibly by 16.4 mg. After cleaning, the mass remained at 4.7 mg. This indicates that a thicker, more adherent passive layer formed and that partial dissolution of the material occurred in parallel with the deposition of compounds on the surface. Figure 2(a) shows that, after one day, the surface is rough, with smooth regions next to rougher areas, probably indicating regions where the α-Zn solution has not yet been completely corroded. This suggests initial, possibly localized, partial corrosion (non-uniform attack).

On the surface, the incipient formation of corrosion products can be observed. These products appear as fine particles or surface deposits and are likely oxides or phosphates (ZnO, $Mg(OH)_2$, or $Zn_3(PO_4)_2$). These structures may act as centers for the formation of the subsequent passive layer. Despite the absence of major visible cracks or exfoliation, the structure appears cohesive, suggesting an early stage of degradation.

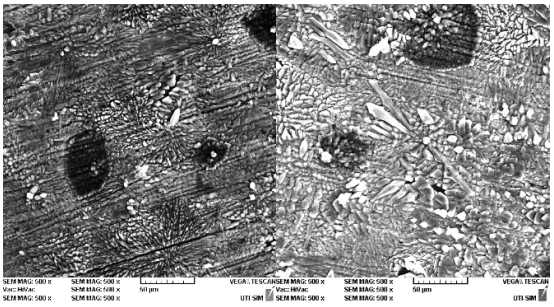

(a) (b)

Fig. 2. SEM images of surface areas of the experimental samples, after (a) one day and (b) three days of immersion.

Figure 2(b) shows the significantly deteriorated surface of the three-day sample. No clean metal areas are visible, indicating that the surface is completely covered. The surface is covered with a compact, textured layer, likely a passive layer of corrosion products. This granular/agglomerated layer consists of aggregated particles, or "nodules," which are typical of Zn and Mg phosphates, as well as oxides (ZnO, MgO).

The texture indicates an active precipitation and growth process of the compounds. In this case, a more advanced degree of corrosion is observed, with a chemically transformed surface and no areas of the original metallic substrate. This indicates the nearly complete dissolution of Zn at the surface, which is replaced by a layer formed from reaction products.

For the sample immersed in DPBS for one day, the analysis of elemental distributions shows clear intensity variations between regions (probably due to Zn and O). These variations indicate partial corrosion, with some regions still exposed to the base metal and others with corrosion products already formed.

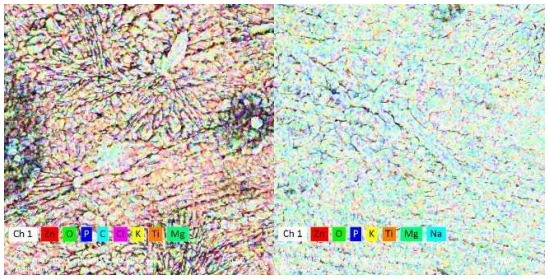

(a) (b)

Fig. 3. The chemical element distribution on the immersed samples in DBPS, after (a) one day and (b) three days of immersion.

Strong contrasts in certain regions may indicate the initial formation of corrosion products, such as oxides or phosphates. These correspond to P- and O-rich regions in the numerical EDS data. Chlorine (Cl) is only mentioned in one area in the table; in the image, it would appear as punctiform spots (if mapped separately), suggesting localized attack (pitting). Additionally, observations of the elemental distribution on the surface of the sample immersed for three days show a much more uniform pattern, with a corrosion layer that appears to cover the entire surface. These results indicate the formation of a well-developed passive layer composed of oxides (ZnO and MgO) and phosphates ($Zn_3(PO_4)_2$ and $Mg_3(PO_4)_2$). Compared to the one-day image (Figure 1(a)), there were no sudden differences in composition, indicating that the reactions had progressed across the surface. The texture of the image suggests a fine mixture of oxides and phosphates rather than punctiform accumulations, reflecting the chemical stabilization of the surface.

The substantial decrease in zinc (Zn) content on the surface (Table 3), from ~96 wt% initially to 46-50 wt% after 1-3 days, indicates Zn dissolution by preferential corrosion. The significant increase in oxygen content (~32 wt%, or 56-58 at%) reflects the formation of oxidized corrosion products, such as ZnO, MgO, TiO_2, and metal phosphates. The detection of phosphorus (~8 wt%) suggests the formation of metal phosphates (e.g., $Zn_3(PO_4)_2$), resulting from a reaction with phosphate ions in the solution. Carbon (C) was detected after one day, but decreased drastically within three days, likely due to initial organic residues or unstable

adsorbed compounds. Chlorine (Cl) was only found in trace amounts after one day, indicating its minor contribution to local corrosion (pitting) at this stage. Sodium (Na) significantly increases after three days, reflecting the adsorption or incorporation of ions from the DPBS into the corrosion products. This behavior can be attributed to the preferential dissolution of Zn, which leaves behind an oxidized surface rich in O and P.

Table 3

Surface chemical composition of ZnMg-Ti alloy after immersion in DPBS.

Element/ Area		1 day-area 1	1 day-area 2	3 days-area 1	3 days - area 2	EDS err%
Zn	wt	50.6	46.5	50.1	46.8	1.4
	at	21.5	19.5	22.18	20.5	
O	wt	32.8	29.9	32.4	31.9	5.1
	at	56.9	51.2	58.7	57	
P	wt	8.9	7.9	7.96	11.3	0.5
	at	8.0	7.0	7.5	10.5	
C	wt	5.01	3.7	0.61	-	2.6
	at	11.6	8.5	0.72	-	
Cl	wt	1.3	-	-	-	0.12
	at	1.04	-	-	-	
K	wt	0.5	0.5	0.22	0.31	0.1
	at	0.4	0.4	0.16	0.22	
Ti	wt	0.45	0.3	0.32	0.3	0.1
	at	0.26	0.16	0.22	0.17	
Mg	wt	0.31	0.5	-	0.63	0.15
	at	0.35	0.6	-	0.74	
Na	wt	-	10.6	8.4	8.73	3.1
	at	-	12.6	10.6	10.9	

At this stage, a passive layer composed of oxides and phosphates forms, which could reduce the subsequent corrosion rate.

Complex interactions are observed between the alloy and the DPBS, including the adsorption of ions (Na, P, and K) and the formation of surface products. The following are the potential chemical reactions that occur on the surface of the ZnMgTi alloy in DPBS: Zn is the predominant metal and has a negative electrochemical potential, so it dissolves easily, and Mg is even more reactive than Zn and undergoes accelerated dissolution. Both reactions are exhibited at varying pH levels. Ti is more inert but forms a thin, passivating oxide layer in the presence of oxygen: $Ti + O_2 \rightarrow TiO_2$. Simultaneously, reactions involving ions in the DPBS occur alongside metal oxidation reactions. For example, phosphate ions (PO_4^{3-} and HPO_4^{2-}) react with dissolved metal ions (Zn^{2+} and Mg^{2+}) to form metal phosphates. For zinc: $3Zn^{2+} + 2PO_4^{3-} \rightarrow Zn_3(PO_4)_2$ (insoluble precipitate). For magnesium (Mg^{2+}), the reaction is: $3Mg^{2+} + 2PO_4^{3-} \rightarrow Mg_3(PO)_2$ (also insoluble). Dissolved oxygen and water favor the formation of oxides or hydroxides. $Zn^{2+} + 2OH^- \rightarrow Zn(OH) \rightarrow ZnO + H_2O$ (by dehydration), and $Mg^{2+} + 2OH^- \rightarrow Mg(OH)$. Additional interactions that may occur are related to the adsorption of ions in solution (Na^+, K^+, and Cl^-), which explains their minor presence in the final composition. Although Cl^- can contribute to localized corrosion (pitting), its limited role here is attributed to its low concentration.

The time-resolved pH increase, the SEM/EDS evidence of O- and P-rich surface layers after 1–3 days, and the negligible net mass change during the first 72 h indicate that corrosion is rapidly self-limiting in DPBS due to the build-up of mixed oxide/phosphate films. Mechanistically, the as-cast microstructure is expected to contain α-Zn with Mg-rich intermetallics (e.g., Mg_2Zn_{11}) and Ti-bearing particles; these features create local galvanic couples where Mg-rich sites act as micro-anodes and the Zn matrix behaves relatively more cathodic. This explains the early-stage alkalinization (O_2 reduction $\rightarrow OH^-$) and the day-2 transient associated with accelerated Mg dissolution (formation of $Mg(OH)_2$), followed by rapid precipitation of phosphates that blanket both anodic and cathodic areas. The literature shows that Ti additions mitigate galvanic severity by quickly passivating as TiO_2 and by interrupting the electronic connectivity of Zn/Mg microcells; similar behavior is consistent with our EDS detection of Ti traces within the product layer and the observed fast passivation. In phosphate-buffered media, the precipitation kinetics is governed by local supersaturation in Zn^{2+}/Mg^{2+} and phosphate species. The measured pH rise promotes dehydration of $Zn(OH)_2$ to ZnO and, critically, the nucleation/growth of hopeite-type zinc phosphates (nominally $Zn_3(PO_4)_2 \cdot xH_2O$) and mixed Zn/Mg phosphates. The more uniform EDS maps after 3 days,

together with the persistence of Na and P signals, suggest that the film evolves from patchy nucleation islands (day 1) to a compact, ion-incorporating phosphate/oxide scale (day 3) that throttles both anodic metal dissolution and the cathodic oxygen-reduction current—hence the plateau in pH and the minimal net mass loss over 72 h.

Regarding benchmarks, published corrosion rates for closely related zinc alloys in simulated physiological media cluster around ~50–80 $\mu m \cdot y^{-1}$: ~50 $\mu m \cdot y^{-1}$ for Zn–Mg with Mg_2Zn_{11}-driven, yet controlled, galvanic degradation in Hank's solution; ~48–58 $\mu m \cdot y^{-1}$ for Zn–Ti binaries as TiO_2-assisted passivation forms; and ~78 $\mu m \cdot y^{-1}$ for a Zn-3Mg-1Ti alloy where Ti reduces galvanic heterogeneity and favors more uniform attack. These values provide a useful yardstick for biodegradable implants. In our case, the first 3 days in DPBS produced virtually no net mass loss and a fully covered surface, pointing to an initially lower effective penetration rate under phosphate-controlled passivation than the above benchmarks; however, because product accumulation led to apparent mass gains (especially by day 20), a precise rate cannot be extracted from the present gravimetry without standardized chemical removal of corrosion products (e.g., ASTM G31) and complementary electrochemical testing (OCP/EIS, polarization). We therefore interpret our results as evidence that galvanic microcells are quickly "choked" by phosphate precipitation kinetics in DPBS, which likely places the early-time corrosion behavior of Zn-3.5Mg-0.5Ti at the low end of the reported range, pending follow-up rate determinations with cleaning protocols and electrochemical methods for direct comparability.

4. CONCLUSIONS

The pH record of DPBS showed a minor increase due to the electrochemical reactions between the Zn/Mg and the water/oxygen contained within the solution. The variation observed around the second day of immersion may be associated with the acceleration of magnesium dissolution, the weakening of the initial passive layer, and/or the increased formation of passive products that consume protons or release hydroxide ions. These changes align with EDS observations and the typical behavior of biodegradable alloys in phosphate-buffered solutions. The increase in mass of the immersed sample after one and three days was caused by the formation of corrosion products (oxides and phosphates). Ultrasonic cleaning revealed that the alloy experienced minimal corrosion during the first three days. These observations support the results from SEM and EDS: the corrosion was self-limiting, and the resulting layer was protective and passive.

In the ZnMgTi experimental alloy, zinc is the most reactive component and corrodes rapidly in a phosphate environment. Oxide and phosphate layers form as a result of chemical reactions with oxygen (O_2) and phosphate (P) ions found in the solution. These layers can provide temporary passive protection. Magnesium (Mg) and titanium (Ti) contribute less; Mg dissolves easily, while Ti remains more inert and is protected in the surface layer. DPBS favors the formation of phosphate compounds, which may partially protect against Zn dissolution.

A more detailed analysis of the results revealed that Zn and Mg dissolution, oxide and phosphate formation, and the onset of a passive layer occurred on the first day of immersion. After three days, partial surface passivation was observed, along with oxide/phosphate accumulation and reactive area reduction. Titanium, as an alloying element, plays a stabilizing role by being inert and participating in the passive layer. The elemental distribution confirmed the clear evolution of corrosion towards a more chemically stable surface with local heterogeneities (areas richer in Na, Cl, and P). During the first 24 hours, corrosion was observed to be active and unevenly distributed, with metallic and oxidized areas still visible. After three days, chemical reactions have covered the entire surface, forming a relatively homogeneous, protective layer. SEM observations correspond with EDS results and pH variation. Corrosion reactions advanced faster during the first two days and then stabilized due to the formation of a protective layer.

Future tests are planned to exceed 20 days of immersion in order to obtain more results and

improve prediction of the degradation process in relation to maintaining the mechanical integrity of the alloy.

5. REFERENCES

[1] Zhang, S., Yuan, P., Wang, X., Wang, T., Zhao, L., Cui, C., *Fabrication and properties of Zn-3Mg-1Ti alloy as a potential biodegradable implant material*, Materials, 15(3), 940, 2022.

[2] Yin, Z., *Microstructural evolution and mechanical properties of Zn-Ti alloys for biodegradable stent applications*, M.S. Thesis, Michigan Technological University, 2017.

[3] Șutic, A.T., Chelariu, R., Cimpoeșu, R., Roman, A.M., Istrate, B., Goanță, V., Benchea, M., Moscu, M., Alexandru, A., Cimpoeşu, N., Zegan, G., *Corrosion Behavior and Mechanical Properties of Zn–Ti Alloys as Biodegradable Materials*, Metals, 14(7), 764, 2024.

[4] Panaghie, C., Zegan, G., Sodor, A., Cimpoeșu, N., Lohan, N.M., Istrate, B., Roman, A.M., Ioanid, N., *Analysis of Degradation Products of Biodegradable ZnMgY Alloy*, Materials, 16, 3092, 2023.

[5] Liu, Y., Du, T., Qiao, A., Mu, Y., Yang, H., *Zinc-based biodegradable materials for orthopaedic internal fixation*, Journal of functional biomaterials, 13(4), 164, 2022.

[6] Venezuela, J., Dargusch, M.S., *The influence of alloying and fabrication techniques on the mechanical properties, biodegradability and biocompatibility of zinc: A comprehensive review*, Acta biomaterialia, 87, 1-40, 2019.

[7] Wang, X., Lu, H., Li, X., Li, L., Zheng, Y., *Effect of cooling rate and composition on microstructures and properties of Zn-Mg alloys*, Trans. Nonferrous Met. Soc. China, 17, s122-125, 2007.

[8] Hussain, M., Ullah, S., Raza, M.R., Abbas, N., Ali, A., *Recent Developments in Zn-Based Biodegradable Materials for Biomedical Applications*, J. Funct. Biomater., 14, 1, 2023.

[9] García-Mintegui, C., Córdoba, L.C., Buxadera-Palomero, J., Marquina, A., Jiménez-Piqué, E., Ginebra, M.P., Cortina, J.L., Pegueroles, M., *Zn-Mg and Zn-Cu alloys for stenting applications: From nanoscale mechanical characterization to in vitro degradation and biocompatibility*, Bioactive materials, 6(12), 4430-46, 2021.

[10] Wang, K., Tong, X., Lin, J., Wei, A., Li, Y., Dargusch, M., Wen, C., *Binary Zn–Ti alloys for orthopedic applications: Corrosion and degradation behaviors, friction and wear performance, and cytotoxicity*, J. mater. sci. technol, 74, 216-229, 2021.

[11] Zhuo, X., Wu, Y., Ju, J., Liu, H., Jiang, J., Hu, Z., Bai, J., Xue, F., *Recent progress of novel biodegradable zinc alloys: From the perspective of strengthening and toughening*, Journal of materials research and technology, 17, 244-69, 2022.

[12] Jin, H., Zhao, S., Guillory, R., Bowen, P.K., Yin, Z., Griebel, A., Schaffer, J., Earley, E.J., Goldman, J., Drelich, J.W., *Novel high-strength, low-alloys Zn-Mg (< 0.1 wt% Mg) and their arterial biodegradation*, Materials Science and Engineering: C, 84, 67-79, 2018.

[13] Liu, X., Sun, J., Yang, Y., Zhou, F., Pu, Z., Li, L., Zheng, Y., *Microstructure, mechanical properties, in vitro degradation behavior and hemocompatibility of novel Zn–Mg–Sr alloys as biodegradable metals*, Materials Letters, 162, 242-5, 2016.

[14] Ji, C., Ma, A., Jiang, J., Song, D., Liu, H., Guo, S., *Research status and future prospects of biodegradable Zn-Mg alloys*, Journal of Alloys and Compounds, 174669, 2024.

[15] Martynenko, N., Anisimova, N., Tabachkova, N., Rybalchenko, G., Shchetinin, I., Rybalchenko, O., Shinkareva, M., Prosvirnin, D., Lukyanova, E., Temralieva, D., Koltygin, A., *Improved Mechanical Properties of Biocompatible Zn-1.7% Mg and Zn1. 7% Mg-0.2% Zr Alloys Deformed with High-Pressure Torsion*, Metals, 13, 1817, 2023.

[16] Pachla, W., Przybysz, S., Jarzębska, A., Bieda, M., Sztwiertnia, K., Kulczyk, M., Skiba, J., *Structural and mechanical aspects of hypoeutectic Zn–Mg binary alloys for biodegradable vascular stent applications*, Bioactive Materials, 6(1), 26-44, 2021.

[17] Șutic, A.-T., Panaghie, C., Paleu, V., Cimpoesu, C., Roman, AM, Coteata, M., Andrusca, L., Badarau, G., Paraschiv, P., Cimpoesu, N., *Wear resistance of as-cast ZnMg-Y biodegradable alloy*, Materials Research Proceedings, 46, 252-259, 2024.

[18] Streza, A., Antoniac, A., Ciocoiu, R., Cotrut, C.M., Miculescu, M., Miculescu, F., Antoniac, I., Fosca, M., Rau, J.V., Dura, H., *In Vitro Studies Regarding the Effect of Cellulose Acetate-Based Composite Coatings on the Functional Properties of the Biodegradable Mg3Nd Alloys*, Biomimetics, 8(7), 526, 2023.

[19] Cojocaru, V.D., Dan, A., Șerban, N., Cojocaru, E.M., Zărnescu-Ivan, N., Gălbinașu, B.M., *Effect of Cold-Rolling Deformation on the Microstructural and Mechanical Properties of a*

Biocompatible Ti-Nb-Zr-Ta-Sn-Fe Alloy, Materials, 17(10), 2312, 2024.
[20] Rizea, A.D., Arva Ungureanu, E.R., Negrea, D.A., Moga, S.G., Abrudeanu, M., Petrescu, M.I., Stefanoiu, R., Haeussler, A., Anghel, D.C., Constantinescu, L.M., *The Influence of Accidental Overheating on the Microstructure and Hardness of the Inconel 718 Alloy*, Applied Sciences, 15(6), 3057, 2025.

Comportmentul privind coroziunea in vitro al unui aliaj biodegradabil ZnMg-Ti în DPBS

Rezumat: Aliajele biodegradabile sunt utilizate din ce în ce mai mult în domeniul medical pentru proceduri care nu necesită implanturi permanente sau perioade lungi de vindecare. Viteza de degradare mai lentă a aliajelor pe bază de Zn comparativ cu aliajele pe bază de Mg permite soluționarea unui număr mai mare de probleme medicale. După obținerea unui aliaj ZnMgTi prin turnare clasică într-un cuptor cu inducție, a fost studiat comportamentul acestuia în soluția salină tamponată cu fosfat Dulbecco (DPBS). Caracterizarea interacțiunii dintre aliaj și DPBS a condus la posibile explicații pentru comportamentul aliajului la coroziune. Aceste ipoteze au fost confirmate prin analiza variației pH-ului soluției, precum și prin analize chimice prin spectroscopie de raze X cu dispersie după energie (EDS), microscopie electronică de baleiaj (SEM) și prin evaluarea pierderii de masă după imersie.

Ramona CIMPOEȘU, PhD Eng., Assoc. Prof., "Gheorghe Asachi" Technical University of Iasi, Faculty of Materials Science and Engineering, ramona.cimpoesu@academic.tuiasi.ro, 41 Dimitrie Mangeron Blvd., 700050 Iasi, Romania
Romeu CHELARIU, PhD Eng., Professor, "Gheorghe Asachi" Technical University of Iasi, Faculty of Materials Science and Engineering, romeu.chelariu@academic.tiasi.ro, 41 Dimitrie Mangeron Blvd., 700050 Iasi, Romania
Alexandra-Tamara ȘUTIC, Eng., PhD student, "Gheorghe Asachi" Technical University of Iasi, Faculty of Materials Science and Engineering, alexandra-tamara.sutic@student.tuiasi.ro, 41 Dimitrie Mangeron Blvd., 700050 Iasi, Romania
Adrian ALEXANDRU, PhD Eng., Assoc. Prof., "Gheorghe Asachi" Technical University of Iasi, Faculty of Materials Science and Engineering, adrian.alexandru@academic.tuiasi.ro, 41 Dimitrie Mangeron Blvd., 700050 Iasi, Romania
Ana-Maria ROMAN*, PhD Eng., Assistant lecturer, "Gheorghe Asachi" Technical University of Iasi, Faculty of Materials Science and Engineering, ana-maria.roman@academic.tuiasi.ro, 41 Dimitrie Mangeron Blvd., 700050 Iasi, Romania
Gheorghe BĂDĂRĂU, PhD Eng., Assoc. Prof., "Gheorghe Asachi" Technical University of Iasi, Faculty of Materials Science and Engineering, gheorghe.badarau@academic.tuiasi.ro, 41 Dimitrie Mangeron Blvd., 700050 Iasi, Romania
Raluca-Maria FLOREA, PhD Eng., Lecturer, "Gheorghe Asachi" Technical University of Iasi, Faculty of Materials Science and Engineering, raluca-maria.florea@academic.tuiasi.ro, 41 Dimitrie Mangeron Blvd., 700050 Iasi, Romania
Cătălin-Andrei ȚUGUI, PhD Eng., Lecturer, "Gheorghe Asachi" Technical University of Iasi, Faculty of Materials Science and Engineering, catalin-andrei.tugui@academic.tuiasi.ro, 41 Dimitrie Mangeron Blvd., 700050 Iasi, Romania
Mihai-Adrian BERNEVIG, PhD Eng., Lecturer, "Gheorghe Asachi" Technical University of Iasi, Faculty of Materials Science and Engineering, mihai-adrian.bernevig@academic.tuiasi.ro, 41 Dimitrie Mangeron Blvd., 700050 Iasi, Romania
Marius TELIȘCĂ, PhD Eng., Lecturer, "Gheorghe Asachi" Technical University of Iasi, Faculty of Hydrotechnical Engineering, Geodesy and Environmental Engineering, marius.telisca@academic.tuiasi.ro, 63-65 Dimitrie Mangeron Blvd, 700050 Iasi, Romania
Nicanor CIMPOEȘU, PhD Eng. Habil., Professor, "Gheorghe Asachi" Technical University of Iasi, Faculty of Materials Science and Engineering, nicanor.cimpoesu@academic.tuiasi.ro, 41 Dimitrie Mangeron Blvd., 700050 Iasi, Romania